J. Eur. Opt. Society-Rapid Publ. 2025, **21**, 3
© The Author(s), published by EDP Sciences, 2025
https://doi.org/10.1051/jeos/2024047
Available online at: https://jeos.edpsciences.org

Journal of the European Optical Society-Rapid Publications

RESEARCH ARTICLE OPEN ACCESS

Ultra-broad Schmidt modes for biphoton states generated by SPDC in the chirped QPM crystals

Jinbao Wang[1,2], Zhan Zheng[2,*], Helin Wang[2,*], and Qiang Lin[2,*]

[1] College of Mechanical Engineering, Zhejiang University of Technology, Hangzhou 310023, China
[2] Zhejiang Province Key Laboratory of Quantum Precision Measurement, College of Physics, Zhejiang University of Technology, Hangzhou 310023, China

Received 8 November 2024 / Accepted 4 December 2024

Abstract. In the realm of quantum optics, the manipulation and characterization of biphoton states hold significant importance for advancing quantum information processing and communication technologies. This study explores the Schmidt decomposition of ultra-broad biphoton states, revealing that most modes are fulfilled with the frequency response points, and certain modes exhibit exceptionally broad Schmidt spectra. These Schmidt modes in frequency domain are significantly reshaped and widened by a crystal at a moderate chirp-rate when pump bandwidth is about several Giga-Hertz.

Keywords: Biphoton, SPDC, Schmidt modes.

1 Introduction

Multimode states are vital resources in quantum optics [1]. Broadband frequency modes/short temporal modes are ideal candidates to take advantage of the multimodality of optical states. To date, ultrashort quantum pulses of few cycle [2–4], single cycle [5–7], and even subcycle [8] levels are successfully generated. Though with some developments in classical theory [9], fundamental tests [10, 11], and ultrafast applications [12–14], subcycle regime of quantum nonlinear optics is still challenging, due to the lack of subcycle sources.

Biphoton states [15], generated by spontaneous parametric down-conversion(SPDC), have the characteristic of nonclassical physics and have been widely studied and applied in theory and experiment. In particular, there is a strong correlation between the signal and idler photons generated in the SPDC process, as well as a high degree of entanglement in space and frequency [16, 17]. It makes them be attractive and widely applied in quantum optics, quantum information and quantum measurement [18, 19]. The broadband of spectrum for the biphoton, reaches the terahertz (THz) in frequency, shows many non-classical physical properties and opens up entirely new perspectives [20–22]. In order to better control and modulate the spatial and spectral characteristics of the biphoton, the method for quantifying the entanglement based on the Schmidt decomposition has been shown in Refs. [23, 24]. The eigenvectors have been reduced single particle density matrices which are named as Schmidt modes. The pure single particle Schmidt mode can be formed with a complete orthogonal basis, and each one can be related with an exact counterpart [25]. Broadband biphoton states are widely generated with short pump pulses in SPDC process [26]. The spectra can be broadened by using chirping quasi-phase matching (QPM) crystals [27], and even with (quasi-) monochromatic pump, the biphoton pulses can be generated at the single cycle level [28, 29] in many Schmidt modes.

2 Theory

To investigate the physical characteristics of biphoton generated by SPDC in the chirped QPM periodically poled lithium niobate (PPLN) crystal, we set a Gaussian pulse with bandwidth ω_p as a pump beam passing through the chirped QPM PPLN crystal, analysis how does the various pump bandwidths and chirped rate influence with the physical characteristics of biphoton in multi-mode during the SPDC process.

As shown in Figure 1a. in a SPDC process inside a linearly chirped QPM PPLN crystal of length L, the poled gratings varying along the propagating z axis, with the alternately opposite poled directions. A photon of a generic frequency ω'_p from a classical strong pump field (central frequency ω_p, bandwidth σ_p) can split in two: a photon of frequency ω and a partner of frequency $\omega'_p - \omega$, and vice

* Corresponding authors: zhan@zjut.edu.cn; whlin@zjut.edu.cn; qlin@zjut.edu.cn

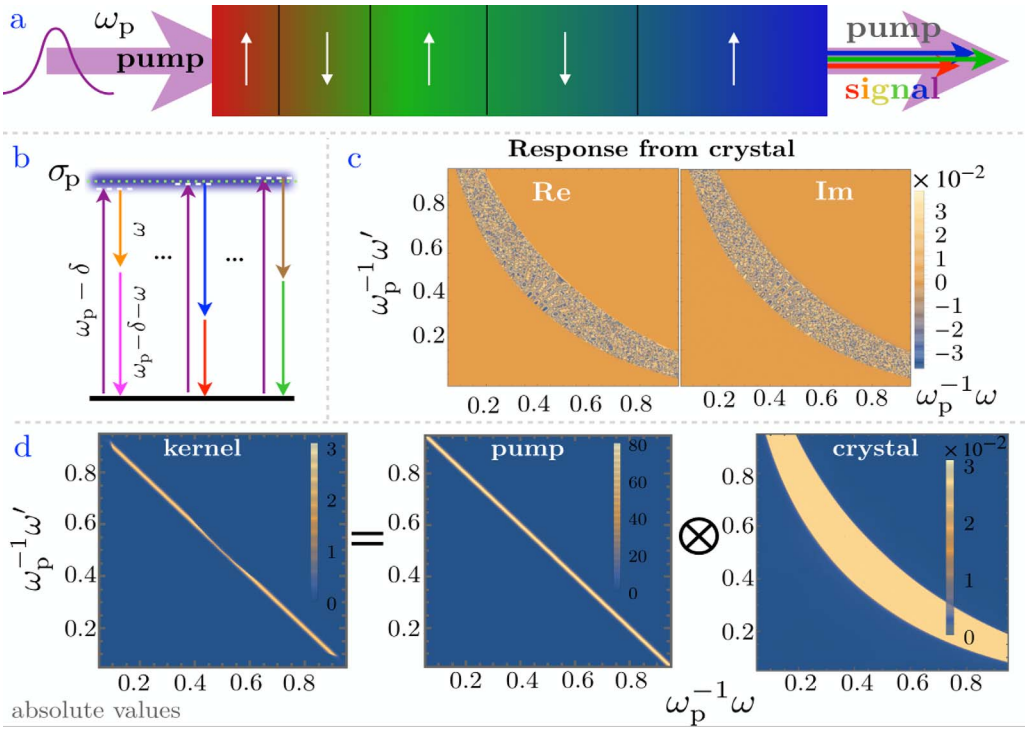

Figure 1. (a) Gaussian pump propagating through the chirped QPM PPLN crystal and splitting into signal and idler pulses during SPDC; (b) Schematic diagram of the down conversion for the pump, signal and idler pulses; (c) The real and imaginary parts for the response function of chirped QPM PPLN crystal; (d) The kernel of the biphoton state amplitude(BSA) function can be viewed as the product of pump function and phase matching function of the crystal.

versa. The spatial frequency of the crystal is $K_0+\zeta z$, where ζ is the chirping parameter, similar to the cases in Refs. [6, 28, 30]. And K_0 is the initial value, which is the poled period in the entrance face of the crystal, matches with the incident pulse frequency $\frac{2\pi}{\Lambda_c}$ to make phase compensation [28]. Following the procedures [26, 29, 31], the biphoton state reads

$$|bi\rangle = T_0 \iint d\omega dw T(\omega, w)\hat{a}^\dagger(\omega)\hat{a}^\dagger(w)|0\rangle. \qquad (1)$$

Here, $\hat{a}^\dagger$ is the creation operator of frequency ω, and T_0 the normalization coefficient. Similar to the assumption in Ref. [28], the pump light can be treated as quasi-monochromatic, the frequency of the pump light can be approximately equal to the sum of the frequencies of the signal and the idler lights. As the Gaussian can be viewed as quasi-monochromatic laser if the bandwidth σ_p is rather narrower compared with the central frequency ω_p of pump light. And the relations between the frequencies for these three pulses associated with σ_p is shown in Figure 1(b). With the conditions of the collinear propagation of the three pulses without consideration for Poynting vector walk-off, we can set this case with noncritical type II QPM configuration [17] and the creation operator $\hat{a}^\dagger$, which operated by the interaction between the pulses with the chirped QPM PPLN, is slowly varying with the distance, and the phase matching function $\Phi(\omega,w)$ can be expressed as follows [28]:

$$\Phi(\omega, w) = \int_0^L \exp\left(\frac{i\zeta z^2}{2} + i\Delta kz\right) dz \qquad (2)$$

where $\Delta k = k(\omega + w) - k(\omega) - k(w) - K_0$ is the phase mismatching involves the phases of the three mixed waves and could be matched with the poled period of the crystal. $k(\omega)$ is the wave-numbers of lights at frequency ω, which is determined by the refractive indices from the Sellmeier equations by $k(\omega) = n\omega/c$.

The biphoton state amplitude(BSA) function $T(\omega,w) = \alpha(\omega,w)\Phi(\omega,w)$ has two parts: the spectral envelope $\alpha(\omega, w) = \sqrt{\frac{1}{\pi\sigma^2}}\exp\left[-\frac{(\omega+w-\omega_p)^2}{2\sigma^2}\right]$, and the phase-matching kernel [6]

$$\Phi(\omega, w) = \frac{\exp\left(\frac{\Delta k(\omega,w)^2}{2i\zeta}\right)}{\sqrt{2\zeta}}\left\{erfi\left[\frac{\zeta L + \Delta k(\omega, w)}{\sqrt{-2i\zeta}}\right] - erfi\left[\frac{\Delta k(\omega, w)}{\sqrt{-2i\zeta}}\right]\right\} \qquad (3)$$

When the chirping parameter ζ is negligibly small, the nonlinear optical processes take place efficiently as some specific frequencies satisfying the conditions $\omega + w = \omega_p$ as well as $\Delta k(\omega, w) = 0$, then the phase-matching kernel becomes sinc functions, which is well-known in the Ref. [32]. However, in general cases, the phase matching kernel can be dramatically different due to the chirping parameter:

the phase-matching kernel is a highly oscillation function for both frequency arguments ω and w in a wide region, giving birth to many fine ripples. Even near the line $\omega + w = \omega_p$, the function $\Phi(\omega, \omega_p - \omega)$ is still highly oscillating, see Figure 1c. As ζz is the compensation of spatial frequency by the crystal, any mismatch $\Delta k(\omega, w)$ from $-\zeta L$ to 0 can fulfill the phase-matching condition $\Delta k(\omega, w) + \zeta z = 0$ at a certain position. As a result, the SPDC processes take place in the active zone $-\zeta L \leq \Delta k(\omega, w) \leq 0$, which can also be known from the properties of Fresnel integral. With larger chirping parameter ζ, more frequencies are allowed to be down-converted from the pump. It allows the phase mismatching with wider frequency range to be compensated, which further expands the frequency response range of the biphoton. One then concludes that the frequencies contribute to the SPDC processes quite equally in the presence of chirp.

The BSA is a function with complicated quadratic phase mismatching factor caused by the interaction between the chirped QPM PPLN crystal and the three waves' phase mismatching. And the chirped QPM plays a substantial roles for this special part. There would be an inevitable ultrabroad response frequency caused by the chirped poled periods for the QPM PPLN crystal.

The BSA function $T(\omega, w)$ can be operated by Schmidt decomposition with the product of the orthogonal eigen basis in the form of ω and w. $T(\omega, w)$ can be expressed by the eigen basis of T written as follows [31]:

$$T(\omega, w) = \sum_n \sqrt{\lambda_n} u_n(\omega) v_n(w) \tag{4}$$

Where λ_n is the eigenvalue corresponding the Schmidt modes u_n and v_n which defined as the eigenvectors for the signal and idler photons.

Schmidt decomposition is expected to quantize calculate the entanglement [17, 31, 33, 34] generated by SPDC. This decomposition process for SPDC involves two factors: the bandwidth of pump pulse and the structure of the nonlinear crystal. For the bandwidth of pump, it means that the frequencies of signal and idler would be independent and not be one-one matching. However, they often show strong correlation for both of them are related to the frequency of pump pulse. The correlation range of frequency for idler light is restricted by the bandwidth of pump light, and the detected signal frequency [34].

The biphoton amplitude is symmetric, $T(\omega, w) = T(w, \omega)$, since $\Delta k(\omega, w) = \Delta k(w, \omega)$. It enables one to make the following Schmidt decomposition

$$T_0\, T(\omega, w) = \sum_{n=1}^{\infty} \sqrt{\frac{\lambda_n}{2}} u_n(\omega) u_n(w)\,, \quad \lambda_1 \geqslant \lambda_2 \geqslant \cdots \geqslant 0 \tag{5}$$

where $\sqrt{\lambda_n}$, $u_n(\omega)$ are known as the Schmidt coefficients and the Schmidt modes respectively, satisfying $\int u_m^*(\omega) u_n(\omega) d\omega = \delta_{mn}$. As a result, the biphoton state can be expressed as

$$|bi\rangle = \sum_{n=1}^{\infty} \sqrt{\lambda_n} |2 : u_n\rangle \tag{6}$$

where $|n : u_k\rangle$ are distinguishable Fock states with n photons in the mode u_k, and the coefficients satisfy $\sum_{n=1}^{\infty} \lambda_n = 1$.

In literature, the Schmidt number $K = 1/\sum_n \lambda_n^2$ is known as a good measure of entanglement in pure biphoton states, and is can also be calculated in the following way

$$K = \frac{\left[\iint |T(\omega, w)|^2 d\omega dw\right]^2}{\iint \left|\int T(\omega, \omega') T^*(\omega', w) d\omega'\right|^2 d\omega dw}. \tag{7}$$

When the spectral bandwidth of the pump is much smaller than the typical distance between two neighboring ripples in the phase-matching kernel, the spectral envelope $\alpha(\omega, w)$ become a narrow peak function along the line $\omega + w = \omega_p$. Because $\alpha(\omega_p - \omega, \omega_p - w) = \alpha(\omega, w)$, the biphoton amplitude should satisfy

$$T(\omega, w) = \simeq T(\omega_p - \omega, \omega_p - w). \tag{8}$$

One may then introduce an analogue of the parity operator $\hat{\beta}$ about the frequency center $\omega_p/2$: $\hat{\beta} f(\omega) = f(\omega_p - \omega)$ for any function f. Because $\hat{\beta}^2 = 1$, the parity operator $\hat{\beta}$ has two eigenvalues ± 1. Consequently, the Schmidt coefficients should be degenerate, and the Schmidt modes can be of odd parity or even parity.

3 Results and analysis

The Schmidt decomposition of wavefunction for biphoton shows a remarkable property that the probability of the particles in Schmidt modes within corresponding condition in the range of 0→100% [33], it means that if the one of pairs photons can be detected in Schmidt mode u_n, and another photon can be detected, within the certain probability in adjoint mode v_n in the same mode index. And the biphoton probability is represented by the $\sqrt{\lambda_n}$ of Schmidt decomposition in the modes $\{u_n, v_n\}$ [33]. The entangled photons can be probed in the homologous modes with certain probability as the entangled one has been detected in the same index. The entanglement can be detected between the two independent frequencies. In this paper, we only consider the pairs in the homologous modes for the two entangled biphoton, the vector value of λ_n represents the paired probability in the same modulus index [31]. Of course some other peculiar parameters such as azimuthal angles which shows orbital angular movement in SPDC configuration has been considered and discussed in Ref. [17], would be ignored in this paper.

Figures 2a–2c shows the Schmidt modes distributions in various cases, one may notice that the Schmidt modes shown in these Figures are symmetrically distributed with the $\omega/\omega_p = 0.5$ and generated biphoton with ultrabroad bandwidth.

It can be found by the simulation that with the appropriate chirp rate, the spectral response frequency $\Delta\omega$ is relatively wide in each Schmidt mode of entangled biphoton generated by SPDC in chirped QPM crystal. The most common structures spectral distribution in Schmidt modes

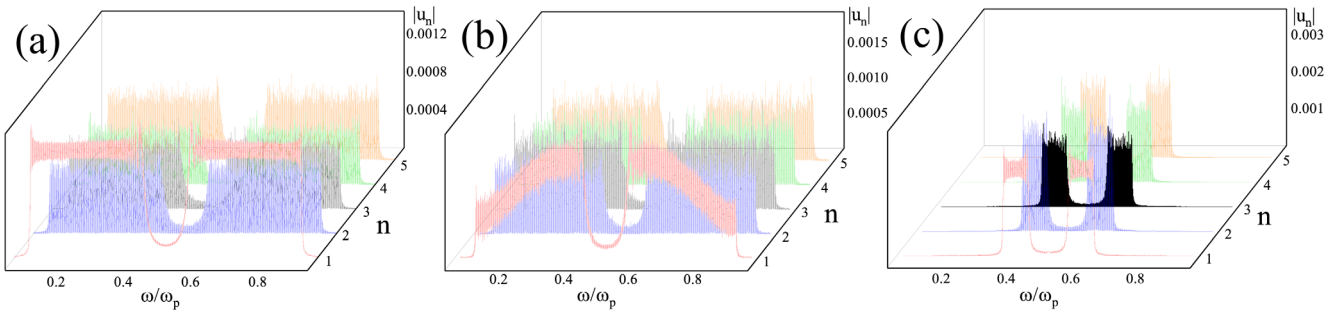

Figure 2. The Schmidt modes distributions with (a) $\sigma_p = 2\pi$GHz and $\zeta = 56$ mm^{-2}; (b) $\sigma_p = 20\pi$GHz and $\zeta = 56$ mm^{-2}; (c) $\sigma_p = 2\pi$GHz and $\zeta = 56$ mm^{-2}. Most modes show the FFRP structures of spectral distribution except $n = 1$.

are filled with full frequency response points(FFRP) distribution. The FFRP distribution represents the response point corresponding to each frequency, but the response amplitude of each point is different, and the amplitude values oscillate between 0 and the maximum value. With some specific conditions, such as when the pumping bandwidth is GHz shown in this paper, the similar structure spectral distribution can be detected in some special Schmidt modes which has been described in Refs. [28, 30].

From Figure 2, it can be found that the distribution of the first mode is clearer and more symmetrical, and its frequency response range $\Delta\omega$ is mainly depended on the chirp rate of the QPM crystal. The chirp rate increase can effectively expand the frequency response range $\Delta\omega$ for the reason of the chirped poled grating periods can effectively compensate the phase mismatching of biphoton with more frequency. By comparison, when the pumping optical bandwidth $\sigma_p = 2\pi$GHz and 20πGHz, its impact on the frequency response range $\Delta\omega$ is not obvious, the main reason is that the center frequency of the pumping optical reaches the THz level, the pumping bandwidth of GHz and 10 GHz is extremely narrow compared with THz, the difference is not particularly obvious, so the impact on the frequency response $\Delta\omega$ is also relatively limited. However, the difference in pumping optical bandwidth will cause the distribution of spectral power in different modes. The main reason is that the bandwidth of the pump laser can affect the frequency relationship between the pump, signal and idler lights. For example, the mode distribution of $n = 1$ in Figure 2 is a very obvious difference. It means that the corresponding amplitudes are larger, with a higher response probability. In particular, when the pumping optical bandwidth $\sigma_p = 2\pi$GHz, the pumping light is closer to the monochromatic light than that at $\sigma_p = 20\pi$GHz. The spectral frequency distribution in this mode is also closer to the biphoton spectral distribution obtained by SPDC with the monochromatic pump light as described in Refs. [28, 30]. The spectrum distribution in the first mode cannot be clearly defined if the pumping bandwidth is too narrow or too wide, and the appropriate pumping bandwidth can be used as an approximation of the monochromatic light, such as σ_p is GHz or 10 GHz levels in the paper. Through the two comparisons, it can be found that when the pumping bandwidth $\sigma_p = 20\pi$GHz, the spectral amplitude of the left and right sides of the generated biphoton with a frequency of $\omega_p/2$ is slightly higher, and the middle of the original double-rectangular distribution is improved.

Table 1. The frequency response bandwidth per central frequency of pump light signed as $\Delta\omega/\omega_p$ in some Schmidt modes

ζ (mm^{-2})	5.6	56	
σ_p (GHz)	2π	2π	20π
Modulus index		$\Delta\omega/\omega_p$	
$n = 1$	0.7191	1.2435	1.2416
$n = 2$	0.7189	1.2410	1.2370
$n = 3$	0.7182	1.2410	1.2370
$n = 4$	0.7172	1.2366	1.2385
$n = 5$	0.7160	1.2406	1.2401

With the increase of the modulus index n, the distribution of each mode shows less different, and the frequency response range $\Delta\omega$ is almost consistent, and all of them fill the entire spectral frequency space. By comparing different Schmidt modes with different pump bandwidths and different chirp rates, it can be found that the main spectral form is FFRP distribution, and the spectral distribution described in Refs. [28, 30] can be obtained only in some specific modes with modulus index $n = 1$ mode, and the other modes are basically FFRP distribution. The frequency response range $\Delta\omega$ is consistent in different modes with the same chirp rate and pump bandwidth. Therefore, a basic conclusion can be drawn that the chirp rate is the main factor affecting the frequency response range in the SPDC of chirped QPM crystals when the pump light is determined.

Table 1 specifically describes the variation of the ratio of spectral response range $\Delta\omega$ to the center frequency of the pump light in different modes with different chirp rates and pumping bandwidth. By comparison, it can be found that the chirp rate of the QPM crystal is the main decisive factor. When the chirp rate is small, the frequency response range $\Delta\omega$ is also narrower, narrower than the center frequency of the pump light. As the chirp rate increases, the frequency response range $\Delta\omega$ becomes wider, even wider than the center frequency of the pump light. Meanwhile,

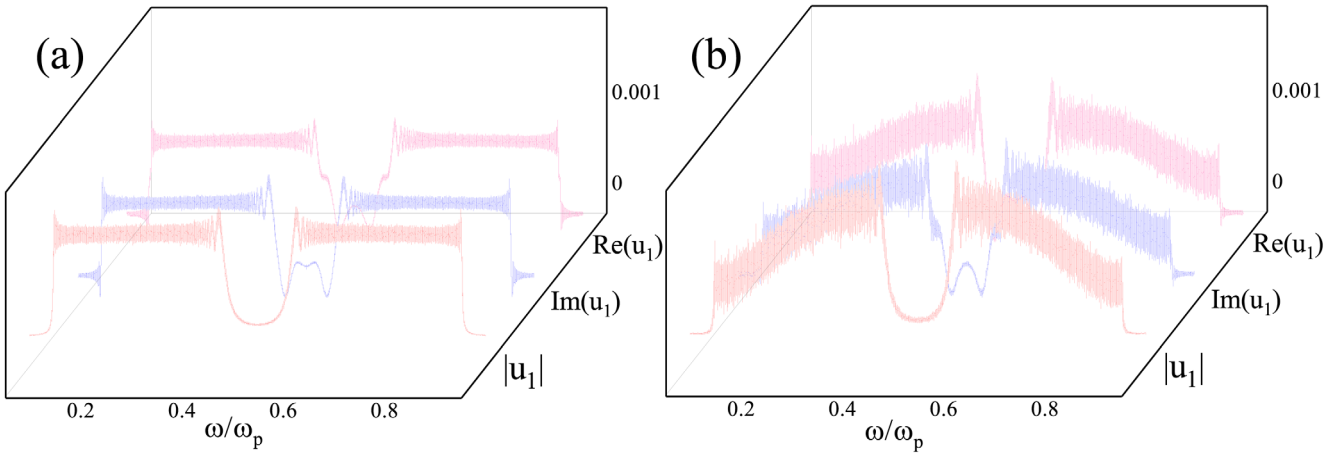

Figure 3. The real and imaginary parts of the Schmidt modes $n = 1$ with the chirp rate $\zeta = 56\ \mathrm{mm}^{-2}$ and the pump bandwidth is set as (a) $\sigma_p = 2\pi$GHz; (b) $\sigma_p = 20\pi$GHz.

the frequency response range $\Delta\omega$ with the same chirp rate and pump bandwidth in different modes are almost consistent. A slightly wider of the frequency response range $\Delta\omega$ could be slightly wider in modulus index $n = 1$, but not particularly obvious.

In the bi-rectangular spectral distribution, the absolute value, the real part and the imaginary part also show similar distributions in this mode (see Fig. 3). There are two main differences: First, at the central frequency $\omega_p/2$, both the real part and the imaginary part slightly oscillate, but for the absolute value, the oscillation part disappears, forming a bi-rectangular spectral distribution similar to that in Refs. [28, 30]. Another difference is that at low frequency and high frequency, both the real and the imaginary parts have spectral distribution, but the distribution oscillates near 0. However, for the spectral distribution in absolute value, the value at low frequency and high frequency becomes 0 again.

4 Conclusion

As the investigation of Schmidt mode distributions for biphoton generated by SPDC in the chirped QPM crystals, theoretical results show that the pulses have rich structures in many modes. Most distributions are fulfilled with the frequency response points. These Schmidt modes in frequency domain are significantly reshaped and widened by the crystal at a moderate chirp-rate. These broadband spectral distributions in Schmidt modes help us to obtain temporal ultrashort pulses with few-, single- or even sub- cycles. The results provide some insights into this special optical process, and can be helpful to quantum technologies.

Acknowledgments

This work was supported by the Joint Funds of the National Natural Science Foundation of China under Grant U2341246. The first author would like to sincerely thank S. E. Harris for his Mathematica codes.

Funding

This work was funded by the Joint Funds of the National Natural Science Foundation of China under Grant U2341246.

Conflicts of interest

The authors declare no conflict of interest.

Data availability statement

Necessary data are included in this article. Other data will be available from the corresponding authors upon reasonable request.

Author contribution statement

Jinbao Wang simulated and calculated this work, and wrote the article. Zhan Zheng and Helin Wang contributed to design and supervise this work. Qiang Lin participated in the discussions about this work and reviewed the manuscript.

References

1 Fabre C, Treps N, Modes and states in quantum optics, *Rev. Mod. Phys.* **92**, 035005 (2020). https://doi.org/10.1103/RevModPhys.92.035005.
2 Wenger J, Tualle-Brouri R, Grangier P, Pulsed homodyne measurements of femtosecond squeezed pulses generated by single-pass parametric deamplification, *Opt. Lett.* **29**, 1267–1269 (2004). https://doi.org/10.1364/OL.29.001267.
3 Pinel O et al., Generation and characterization of multimode quantum frequency combs, *Phys. Rev. Lett.* **108**, 083601 (2012). https://doi.org/10.1103/PhysRevLett.108.083601.
4 Iskhakov T et al., Generation and direct detection of broadband mesoscopic polarization190 squeezed vacuum, *Phys. Rev. Lett.* **102**, 183602 (2009). https://doi.org/10.1103/PhysRevLett.102.183602.
5 Shverdin MY et al., Generation of a single-cycle optical pulse, *Phys. Rev. Lett.* **94**, 033904 (2005). https://doi.org/10.1103/PhysRevLett.94.033904.
6 Nasr MB et al., Ultrabroadband biphoton generated via chirped quasi-phase-matched optical parametric down-conversion, *Phys. Rev. Lett.* **100**, 183601 (2008). https://doi.org/10.1103/PhysRevLett.100.183601.

7 Sensarn S, Yin GY, Harris SE, Generation and compression of chirped biphoton, *Phys. Rev. Lett.* **104**, 253602 (2010). https://doi.org/10.1103/PhysRevLett.104.253602.

8 Riek C et al., Subcycle quantum electrodynamics, *Nature* **541**, 376–379 (2017). https://doi.org/10.1038/nature21024.

9 Lin Q, Zheng J, Becker W, Subcycle pulsed focused vector beams, *Phys. Rev. Lett.* **97**, 253902 (2006). https://doi.org/10.1103/PhysRevLett.97.253902.

10 Kizmann M et al., Subcycle squeezing of light from a time flow perspective, *Nat. Phys.* **15**, 960–966 (2019). https://doi.org/10.1038/s41567-019-0560-2.

11 Guedes TLM et al., Spectra of ultrabroadband squeezed pulses and the finite-time unruh-davies effect, *Phys. Rev. Lett.* **122**, 053604 (2019). https://doi.org/10.1103/PhysRevLett.122.053604.

12 Günter G et al., Sub-cycle switch-on of ultrastrong light–matter interaction, *Nature* **458**, 178–181 (2009). https://doi.org/10.1038/nature07838.

13 Schubert O et al., Sub-cycle control of terahertz high-harmonic generation by dynamical bloch oscillations, *Nat. Photonics* **8**, 119–123 (2014). https://doi.org/10.1038/nphoton.2013.349.

14 Carlson DR et al., Ultrafast electro-optic light with subcycle control, *Science* **361**, 1358–1363 (2018). https://doi.org/10.1126/science.aat6451.

15 Shih Y, Entangled biphoton source-property and preparation, *Rep. Prog. Phys.* **66**, 1009–1044 (2003). https://doi.org/10.1088/0034-4885/66/6/203.

16 Iskhakov TS et al., Polarization-entangled light pulses of 105 photons, *Phys. Rev. Lett.* **109**, 150502 (2012). https://doi.org/10.1103/PhysRevLett.109.150502.

17 Svozilík J, Peřina J, Torres JP, High spatial entanglement via chirped quasi-phase-matched optical parametric down-conversion, *Phys. Rev. A* **86**, 052318 (2012). https://doi.org/10.1103/PhysRevA.86.052318.

18 Brida G et al., Detection of multimode spatial correlation in pdc and application to the absolute calibration of a ccd camera, *Opt. Express* **18**, 20572–20584 (2010). https://doi.org/10.1364/OE.18.020572.

19 Agafonov IN, Chekhova MV, Leuchs G, Two-color bright squeezed vacuum, *Phys. Rev. A* **82**, 011801 (2010). https://doi.org/10.1103/PhysRevA.82.011801.

20 Kitaeva GK et al., Generation of optical signal and terahertz idler photons by spontaneous parametric down-conversion, *Phys. Rev. A* **98**, 063844 (2018). https://doi.org/10.1103/PhysRevA.98.063844.

21 Haase B et al., Spontaneous parametric down-conversion of photons at 660 nm to the terahertz and sub-terahertz frequency range, *Opt. Express* **27**, 7458–7468 (2019). https://doi.org/10.1364/OE.27.007458.

22 Kuznetsov KA et al., Nonlinear interference in the strongly nondegenerate regime and schmidt mode analysis, *Phys. Rev. A* **101**, 053843 (2020). https://doi.org/10.1103/PhysRevA.101.053843.

23 Arnaut HH, Barbosa GA, Orbital and intrinsic angular momentum of single photons and entangled pairs of photons generated by parametric down-conversion, *Phys. Rev. Lett.* **85**, 286–289 (2000). https://doi.org/10.1103/PhysRevLett.85.286.

24 Law CK, Eberly JH, Analysis and interpretation of high transverse entanglement in optical parametric down conversion, *Phys. Rev. Lett.* **92**, 127903 (2004). https://doi.org/10.1103/PhysRevLett.92.127903.

25 Straupe SS et al., Angular schmidt modes in spontaneous parametric down-conversion, *Phys. Rev. A* **83**, 060302 (2011). https://doi.org/10.1103/PhysRevA.83.060302.

26 Dayan B, Theory of two-photon interactions with broadband down-converted light and entangled photons, *Phys. Rev. A* **76**, 043813 (2007). https://doi.org/10.1103/PhysRevA.76.043813.

27 Jovanovic I, Ebbers CA, Barty CPJ, Hybrid chirped-pulse amplification, *Opt. Lett.* **27**, 1622–1624 (2002). https://doi.org/10.1364/OL.27.001622.

28 Harris SE, Chirp and compress: toward single-cycle biphoton, *Phys. Rev. Lett.* **98**, 063602 (2007). https://doi.org/10.1103/PhysRevLett.98.063602.

29 Horoshko DB, Kolobov MI, Generation of monocycle squeezed light in chirped quasi-phase-matched nonlinear crystals, *Phys. Rev. A* **95**, 033837 (2017). https://doi.org/10.1103/PhysRevA.95.033837.

30 Horoshko DB, Kolobov MI, Towards single-cycle squeezing in chirped quasi-phase-matched optical parametric down-conversion, *Phys. Rev. A* **88**, 033806 (2013). https://doi.org/10.1103/PhysRevA.88.033806.

31 Law CK, Walmsley IA, Eberly JH, Continuous frequency entanglement: effective finite hilbert space and entropy control, *Phys. Rev. Lett.* **84**, 5304–5307 (2000). https://doi.org/10.1103/PhysRevLett.84.5304.

32 Horoshko DB et al., Bloch-messiah reduction for twin beams of light, *Phys. Rev. A* **100**, 013837 (2019). https://doi.org/10.1103/PhysRevA.100.013837.

33 Fedorov M, Miklin N, Schmidt modes and entanglement, *Contemp. Phys.* **55**, 94–109 (2014). https://doi.org/10.1080/00107514.2013.878554.

34 Grice WP, U'Ren AB, Walmsley IA, Eliminating frequency and space-time correlations in multiphoton states, *Phys. Rev. A* **64**, 063815 (2001). https://doi.org/10.1103/PhysRevA.64.063815.